International Journal of Automotive and Mechanical Engineering
ISSN: 2229-8649 (Print); ISSN: 2180-1606 (Online);
Volume 14, Issue 1 pp. 3849-3871 March 2017

DOI: https://doi.org/10.15282/ijame.14.1.2017.4.0314

Morphological analysis of injected sprays of different bio-diesel fuels by using a common rail setup controlled by a programmable electronic system

P. Visconti*, P. Primiceri, L. Strafella, A.P. Carlucci and A. Ficarella

Department of Innovation Engineering, University of Salento – 73100 Lecce, Italy
*Email: paolo.visconti@unisalento.it

ABSTRACT

Biodiesel fuels are increasingly attracting interest in the scientific community and in the world motor industry. The morphological analysis of injected sprays is a key factor to increase engine performances using new biodiesel fuels and to compare them with those related to the use of conventional fuels. In this paper, an experimental setup is realised to carry out test campaigns, in order to analyse and compare the spray injections of different fuel typologies. A PC-interfaced electronic system was realised for driving *BOSCH* injectors and for varying the injection pressure and opening time. Hence, the morphological analysis was performed for each tested fuel by characterising the shape-ratio and penetration depth inside the velocimetric chamber. The results show higher penetration values for biodiesel fuels due to their viscosity and drops in superficial tension, which facilitate a deeper penetration compared to those obtained with conventional diesel fuels. Although used biodiesels contain only 20% of renewable vegetable-origin diesel fuels, the viscosity and superficial tension are slightly higher than those of petroleum diesel, thus determining a weak vaporisation and formation of larger drops. By knowing the morphological behaviour of sprays using biofuels and conventional fuel, it is possible, by using programmable electronic systems, to adjust and improve the spray parameters in order to obtain better engine performances. The results reported in this instance could be utilised by future research works for choosing the most suitable biofuel based on the desired morphological behaviour of the injected sprays.

Keywords: Biodiesel fuels; spray characterisation; common rail system; electronic injector driving, measurements, experimental setup.

INTRODUCTION

In these last years, biodiesel fuels have been attracting more and more interest in the scientific community and in the world motor industry, constituting clean biodiesel, biodegradable and renewable fuels. Numerous experimental studies have already been conducted on the combustion and emissions of biodiesel fuel in conventional diesel engines [1-5]. Biodiesel is a liquid and transparent fuel, with an amber colour, entirely obtained from renewable sources such as vegetable oil (rapeseed, sunflower or other), produced by dedicated oil crops, from exhausted oils and food-borne animal/vegetable fats; the latter can be recovered through waste recycling, coming, for example, from the restaurant business, food processing industries and households [6-9]. Biodiesel fuels are produced through a trans-esterification reaction, i.e. a process in which a vegetable oil is reacted in an excess of methyl alcohol in the presence of an alkaline catalyst; the final product is a mixture of a few methyl esters with the absence of sulphur and aromatic compounds. It contains oxygen in a high amount (not less than 10%); its viscosity is

slightly higher to that of the conventional diesel and it can be used, mixed with diesel fuel or not, as fuel for transport and heating [10].

Compared to conventional diesel, biodiesel presents a better performance; it makes it possible to obtain a faster ignition, because of a higher cetane number than the conventional diesel and a more complete combustion of fuel charge which means fewer black smoke emissions during start-up and normal operation. On the contrary, biodiesel is more perishable and it has a lower energy density compared to conventional diesel; in fact, in order to replace 1kg of conventional diesel, 1,13 kg of biodiesel are needed [11-14]. However, considering the whole chain of biofuel production, the emission of polluting gases in the atmosphere is significantly reduced using the biodiesel fuel rather than the fossil fuel [15-19]. At the Italian latitudes, the employed dedicated crops for biodiesel production are generally rapeseed, sunflower and, to a lesser extent, soybean. In the southern regions, the Brassica Carinata represents a relatively promising crop due to its modest water requirements and high degree of adaptability to soils [20]. In addition to oils derived from dedicated crops, the so-called second-generation biofuels must also be taken into account; for example, they can be produced from a ligno-cellulosic biomass at very low costs. Even if the production technologies are still not optimised, second-generation biofuels are considered very promising because they make it possible to reduce the product costs of biofuel, compared to those for producing first-generation biodiesel and diesel from fossil fuel, a key factor for a greater spread of biodiesel [21]. Between second-generation biofuels, there is biodiesel resulting from coffee; the coffee wastes can become a viable alternative to first-generation fuels, fully entering into the second generation; in fact, these biofuels do not subtract land to food crops and avoid damage to biodiversity with intensive crops [22]. In this research work, the biofuels used for the morphological study of the injected sprays are shown in the bottles in Figure 1. Besides coffee, they are also derived from the Cynara cardunculus and from the Brassica carinata and are blended, each of them, with petroleum diesel in percentage equal to 20%, in order to obtain B20 biodiesel fuels.

Figure 1. Coffee beans on the right and used biodiesel fuels derived from the Cynara cardunculus (orange colour), Brassica carinata (yellow colour) and Coffee (black colour) in the bottles on the left.

Cynara cardunculus and Brassica carinata are an environmentally friendly alternative and also more fruitful than traditional crops for energy production from biomass and biofuels. This typology of green-energy, produced from vegetal oil, not only avoids subtracting land to food crops but also allows the recovery of abandoned areas (marginal or seeds-marginal soils). Furthermore, the by-product resulting from Cynara

cardunculus bio-liquids, i.e. the lignin, can replace carbon and thus also contributes to the energy needs from biomass [23]. The employment of pure vegetable oils in the internal combustion engine can lead to engine operating problems caused mainly by the higher viscosity of vegetable oils than conventional diesel fuels. The injection quality depends on the fuel viscosity; a higher viscosity results in a lower oil pulverising in the combustion chamber causing a more difficult combustion and residue formation. However, modern biodiesel mixed with conventional diesel up to 30% by volume, can be used today in most engines without any modification to the fuel system. The use of pure biodiesel is possible only for certain specific engines, whereas for others some technical adjustments are necessary. The Common Rail system provides a direct injection of an amount of fuel inside the cylinder [24-27]. Because of the low fuel volatility and the reduced time for carrying out the combustion process in compression ignition engines, the pulverisation of the fuel sprays and the air-fuel mixing play a key role in the engine performance, from combustion to exhausting emissions [28-36]. In this context, the automotive world is evaluating the possibility to use biofuels in substitution to the traditional diesel. In addition, this is efficient in order to obtain better biodiesel characteristics, such as minor density and viscosity variations, lower aromatic hydrocarbons content and a more convenient sprays morphology of the injected biofuel inside the combustion chamber [37-41]. Hence, in this research work, the results of different tests performed in order to characterise the sprays morphology provided by a diesel injector, varying injection pressure and opening time, are shown; four fuel typologies were tested, three types of biodiesel and the conventional diesel [42-49]. Using a fast camera, the images related to spray injections were acquired and post-processed using a LabVIEW software, thereby characterising each injected spray related to a particular fuel typology and comparing the morphology (spray penetration depth and shape ratio) of the different performed injections for each tested fuel. A morphological analysis of different biofuels has been performed comparing it with that related to conventional diesel; the obtained results show a deeper penetration for biodiesel fuels than conventional diesel. In fact, as confirmed by other studies, due to a weak vaporisation with a consequent formation of drops with larger diameter, the sprays penetration for biodiesel fuels reaches higher values than conventional diesel [22], [23]. The proper functioning of the realised programmable electronic system was tested, promoting it as a good candidate to be used for diesel injectors in test benches in which the injection parameters have to be changed. By knowing the chemical composition of used biofuels, it is possible to use some biofuels rather than others to obtain the desired morphological behaviour inside the velocimetric chamber. Moreover, based on the results reported herein, future research works can identify biofuels featured by the desired morphological behaviour to be used for improving the engine performances and fuel consumption, as a function of the specific application.

EXPERIMENTAL SETUP

Modelling Specifications

In order to characterise the sprays morphology of different types of fuel, i.e. conventional diesel and biofuels mixed with it (B20), the experimental setup shown in Figure 2 was realised. The aim of this work is the spatial and temporal analysis, in terms of penetration and shape ratio, of the injected fuel by varying the injection parameters, i.e. injection pressure and time duration, with constant back-pressure in the quiescent chamber (filled

with inert gas, nitrogen in our case). The main components of the realised setup are described below.

i) *Mechanical and hydraulic system (orange section)*: the Common Rail system is composed of a high pressure hydraulic circuit, realised with a high pressure pump, a common accumulator (rail) and various pipes, and of a low pressure section with a proper pump, several filtering stages and ducts. It is provided with a pressure regulator, a pressure sensor, the *Bosch* injector and a velocimetric chamber with optical accesses.

ii) *Memrecam for injection recording in the velocimetric chamber (blue section):* the velocimetric chamber is provided with two quartz lateral accesses to illuminate it in order to make it possible to capture high quality spray images using the *MemrecamGXlink* placed in front of chamber (where a third optical access is present), as shown in Figure 2. The adopted procedure to record the spray pattern with proper synchronisation between the injector, Memrecam and other components of the experimental setup will be described later.

iii) *Electronic apparatus(red section):* this section is composed of a PC for managing of the injection operation making use of a LabVIEW Virtual Instrument that drives the NIUSB-6259 acquisition board; the TTL control signals are generated as input to the suitably realised electronic board for injector driving, synchronised with the video-camera trigger signal for recording the injection process in the velocimetric chamber.

Before describing the subsequent procedure for recording the injection process, the realised electronic control units and the used Bosch injector are described below.

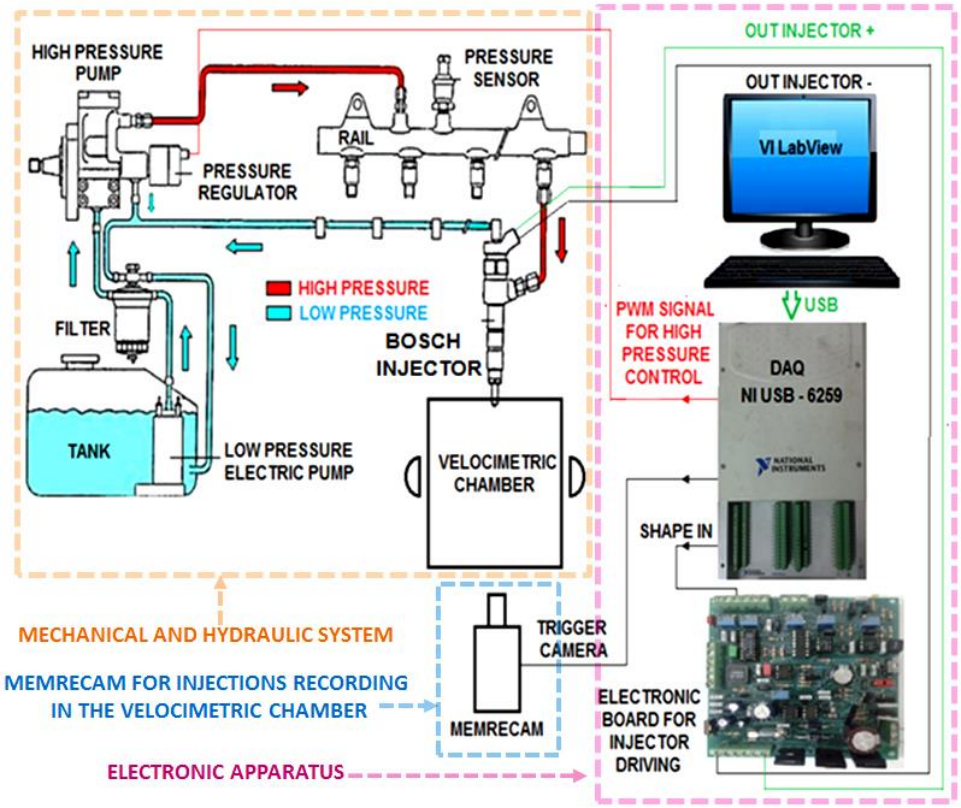

Figure 2. Block scheme of the experimental apparatus: replicated Common Rail system in the orange section, memrecam in the blue section and PC/electronic control units in the red section.

Electronic Board for Injector Driving

In Figure 3(a), the used injector *BOSCH 0445110266-825* is reported; it needs suitable voltage and current signals, as shown in Figure 3(b), for a proper operation. These signals are provided from the control/driving board, shown in Figure 4(a), which transforms a 0-5V signal, named *Shape in* or *Energizing Time* (the high level injection command with a duration of 140 μs ÷ 2 ms, reported in the upper section in Figure 3(b)) in a proper voltage signal (Figure 3(b) at the centre) applied across the inner coil of the injector inductive load. In this way, a current with a shape shown in the bottom of Figure 3(b), flows through the injector coil; the resulting magnetic field determines the lift of the injector atomizer needle, for a time set by the *Shape in* duration, thus obtaining the fuel injection in the velocimetric chamber.

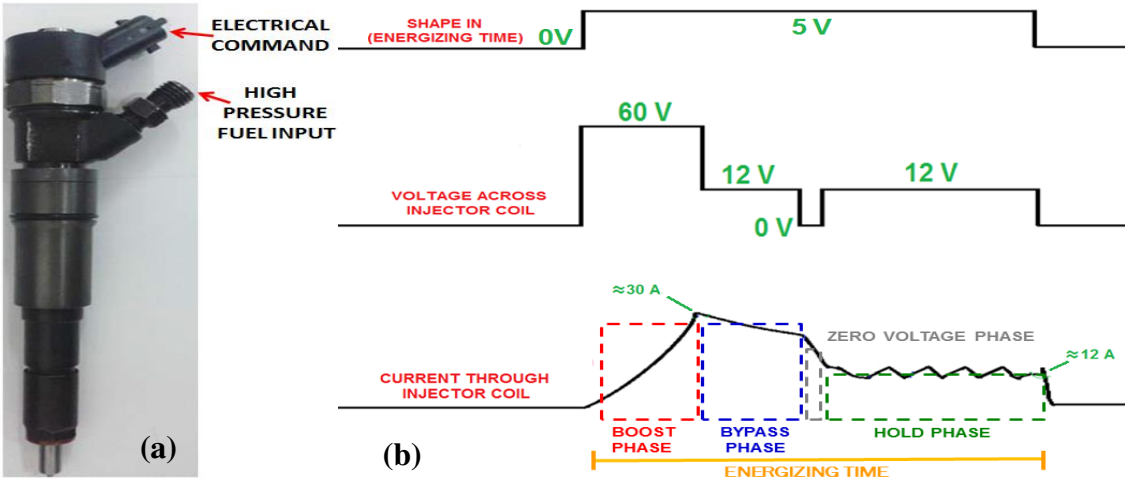

Figure 3. (a) Photo of the used solenoid diesel injector and (b) voltage and current signals, provided from the designed electronic board for proper injector driving.

The current signal presents an initial *Boost Phase*, highlighted in red in Figure 3(b), with a maximum intensity of ≈30A (this *Boost Phase* is required to overcome the intrinsic mechanical forces of the injector, which resist the lift of the needle). After a *Bypass Phase* (blue colour) with a reduced current intensity and a *Zero Voltage Phase* (grey colour) in which the voltage across the inductive load drops to 0V, a *Hold Phase* (green colour) follows, with a current value of ≈12A in order to keep open the injector until the end of the *Shape-in* high level. During the hold and boost phases, a current regulation by means of a feedback circuit is performed. The electrical/temporal injection parameters can be modified acting on six potentiometers highlighted in Figure 4(a). In Figure 4(b), the complete block diagram of the designed electronic driving board with the most significant components is reported. Block 1 is composed of the power supply circuit, of the high voltage section and of a DC-DC step-up converter that elevates the input voltage (12V DC) into a DC output voltage V_{STEPUP} in the range [38.4V - 68.4V]. Through a 0 – 12V PWM signal, with the duty cycle regulated by acting on R_{38} potentiometer, the V_{STEPUP} voltage reaches, in a few instants, the desired value. The output voltages of block 1, 12V DC and adjustable V_{STEPUP}, are provided as inputs to the circuital block 3.

Circuital block 2 is composed of the processing circuit of the command signal for opening/closing the injector (a 0-5V shape-in pulse with variable duration shown in Figure 5(a)) and of the circuital section that provides two 0-5V pulses with an adjustable duration (*Short Pulse*, shown in Figure 5(b), duration in the range [32.9 μs - 172.9 μs],

and *Long Pulse*, Figure 5(c), duration in the range [168 µs – 518 µs]), through the 20 kΩ R_{40} and 50 kΩ R_{29} potentiometers, respectively. Block 2 also includes the generation circuit of the 5-0V T_{OFF} pulse (Figure 5(d)) (duration [10.8 µs ÷ 30.8 µs]), acting on the 20 kΩ R_{24} potentiometer.

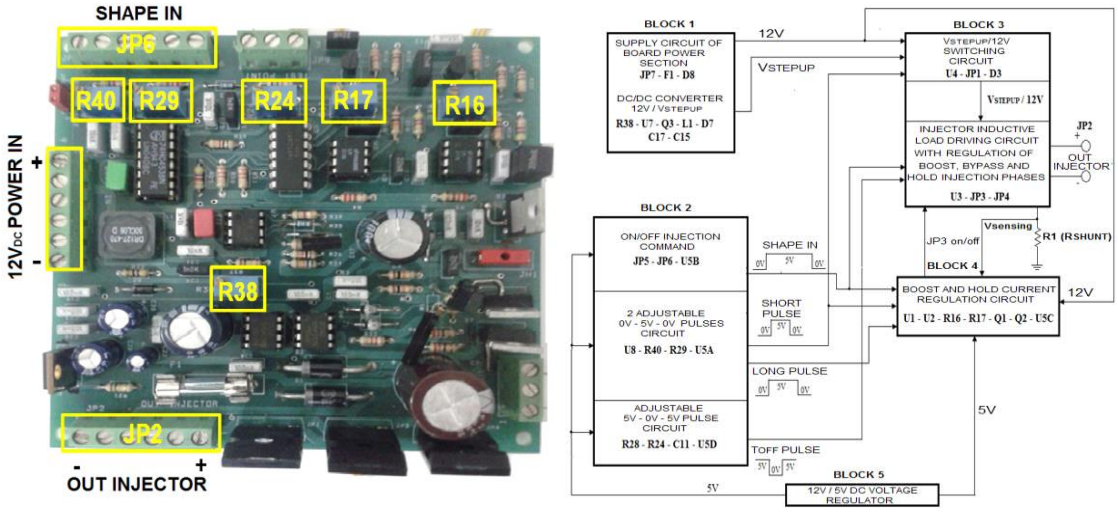

(a) (b)

Figure 4. (a) Electronic board for injector driving with indication of the I/O terminals and potentiometers to adjust the injection parameters; (b) block diagram of the driving board.

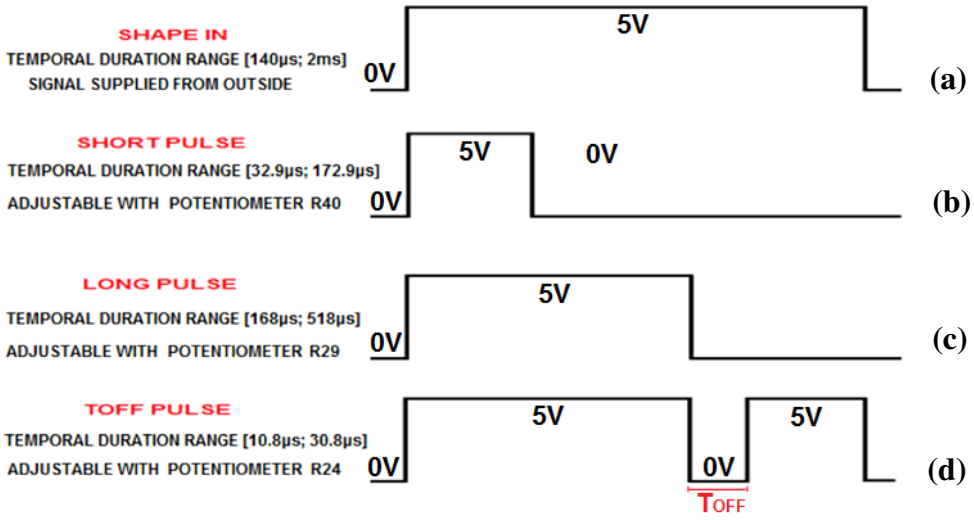

Figure 5. Digital timing signals provided by the circuital block 2.

The *Short Pulse*, *Long Pulse* and T_{OFF} digital signals, together with *Shape in*, are the inputs of blocks 3 and 4 allowing to generate the output voltage signal across the Out Injector terminal and to regulate the operation of the current limitation circuit that flows through the injector load. Block 3 performs various operations: it commutes from 12V to the V_{STEPUP} voltage for the Short Pulse duration and from V_{STEPUP} to 12V when the Short Pulse ends, thus providing by means of switches, 12V or V_{STEPUP} to the Out Injector+ positive terminal, disconnecting these voltages when the current limiting circuit

intervenes. It also provides a path to ground to the injector's current for a time interval equal to the Long Pulse duration, determining after, during the T_{OFF} pulse, a voltage drop across the injector load equal to 0V. In this way, block 3 represents the driving circuit of the inductive injector with a proper time sequence of the *Boost-Bypass-Zero Voltage-Hold* phases. Block 4 is constituted by the regulation circuits of the boost / hold currents flowing through the injector, disconnecting the voltage applied to the injector terminals, if the current value is greater than a threshold value (adjustable via the 10kΩ R_{16} (R_{17}) potentiometer); in this way, an instant drop to 0V of the voltage across the injector occurs causing a current decrease. When the current returns below the threshold value, then the voltage is connected again across the injector, determining a current increase through the inductive load.

Digital Potentiometers to Adjust the Parameters of the Injector Driving Signals

In order to avoid the manual changing of the potentiometer values, a new solution was adopted employing digital potentiometers; in this way, it is possible to modify the electrical/temporal parameters directly from a PC by a suitable interface program. Thus, by removing the mechanical potentiometers, the installed digital potentiometers, through the SPI interface and a microcontroller, are programmed with the proper value related to the desired electrical/temporal parameter of the injector signal. The block scheme of the realised system with the mechanical potentiometers removed is shown in Figure 6.

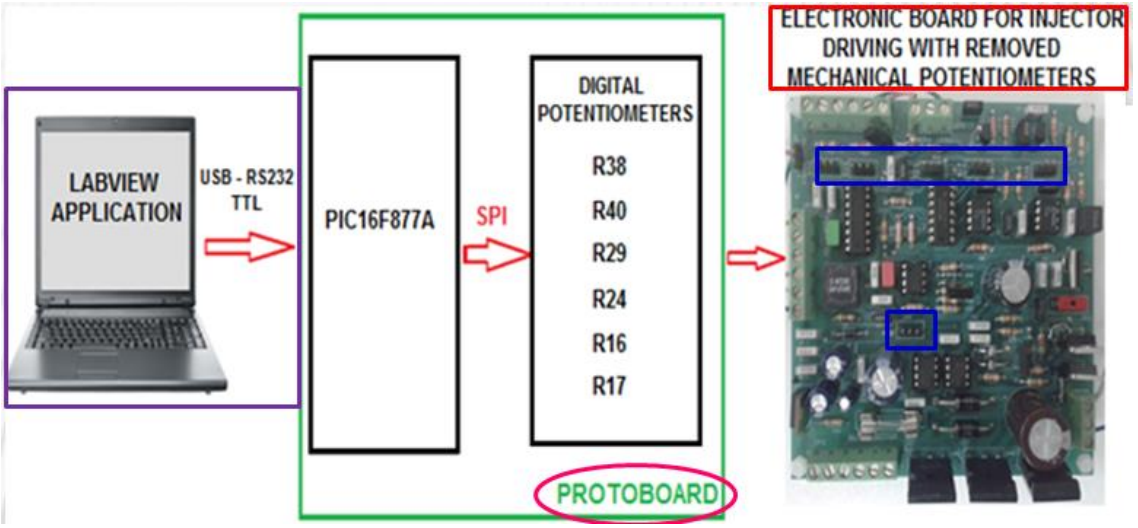

Figure 6. Block scheme of the electronic system to manage the injector parameters from a PC.

The developed solution allows the user to program comfortably the potentiometer's value avoiding the manual intervention and thus to make significant errors in the setting of the mechanical potentiometer value. The electrical scheme of the realised circuit, shown in Figure 7, includes the microcontroller *PIC16F877A* (section 1 in red), 33010 SMT–DIP adapter used for assembling a high voltage digital potentiometer (model *AD5290* from Analog Devices) powered by the 12V–30VSTEP-UP converter (model *12D15NNL* provided from YDS), section 2 in orange, and finally the digital potentiometers (model *MCP41010* and *MCP41050* from Microchip), section 3 in violet. Section 4 in blue is relative to the USB-PC serial communication and to the power supply of the PIC and MCP potentiometers; lastly, a circuit for the voltage stabilisation is present.

The digital potentiometer relative to the adjustment of the DC V_{STEPUP} voltage, used in place of R_{38}, must be able to tolerate a maximum voltage of 30V on its terminals. In order to provide this supply voltage, a STEP–UP 12V–30V DC converter (model *19D-12D15NNL* from YDS), shown in Figure 8(a), was used. The block diagram of the used digital potentiometer, model *AD5290* from Analog Devices, is shown in Figure 8(b); the 50kΩ R_{AB} resistance between the A and B terminals is highlighted in red and the R_{WB} resistor value changes as a function of the programming value inserted from the user on the PC. The MCP41050 potentiometers were employed in the rheostat configuration in place of mechanical potentiometers R_{40} R_{29} and R_{24} (R_{AB}= 50 kΩ). For potentiometers R_{16} and R_{17} relative to the adjustment of the threshold voltages for peak and maintenance currents limitation, the digital potentiometers *MCP41010*with R_{AB}=10 kΩ, in the resistor divider configuration, were used. For all employed potentiometers, it is possible to program 256 resistance values, being the programming digital word composed of 8 bits.

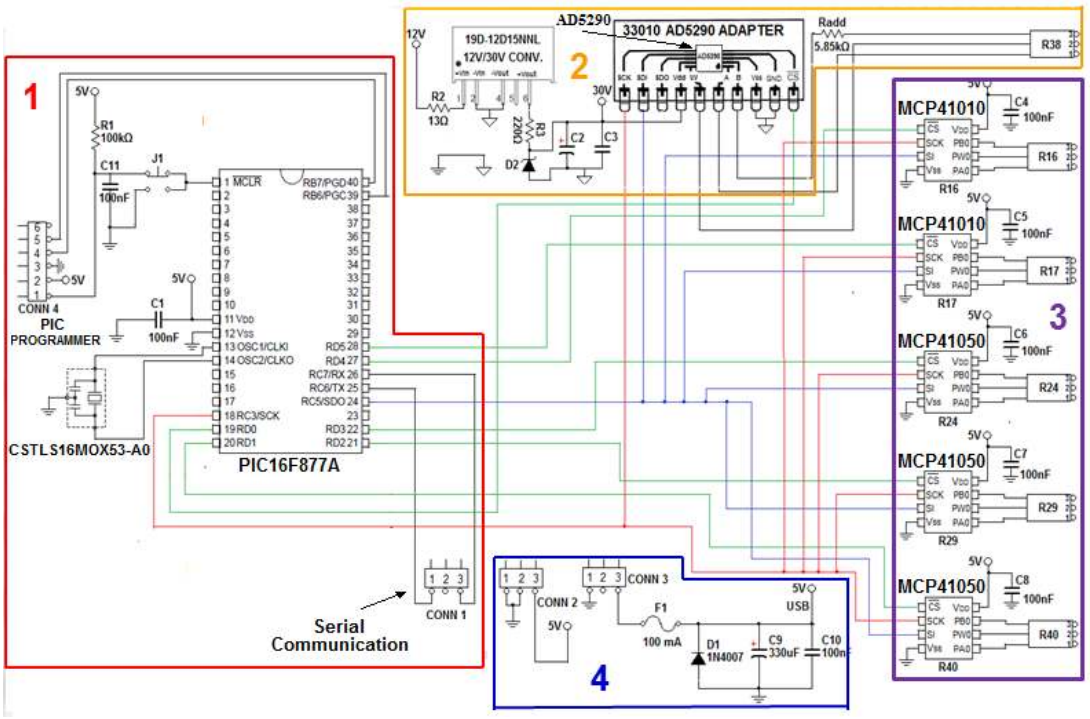

Figure 7. Electrical scheme of the realised prototype board with the indication of the different sections related to the microcontroller, potentiometers and power supply.

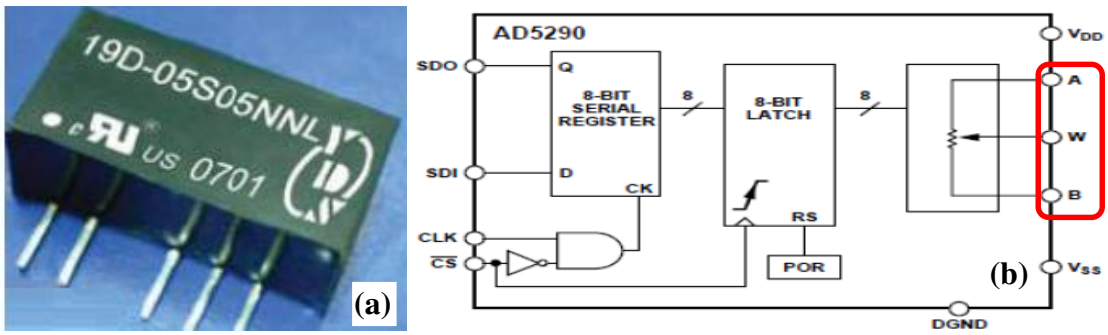

Figure 8. View of the STEP–UP 12V–30V DC converter (a) and inner block diagram of the high voltage digital potentiometer AD5290 (b).

Firmware Development and Testing of the Realised Prototype

The firmware for managing the serial communication between the PC and the microcontroller and for the programming of the digital potentiometers, via the SPI protocol, was developed in the C++ language. In Figure 9, the related flow chart is reported; the user can choose to set the potentiometer values for all potentiometers or for only one of them, by entering '0' or '1' by the keyboard, respectively. Once the programming mode has been chosen, the user has to insert a decimal value between 0 and 255 that corresponds to the desired resistance value; for example, if the R_{38} potentiometer is chosen, the user inserts a value between 0 and 224 which corresponds to a R_{38} resistance value in the range [0kΩ; 44kΩ]. The electrical/temporal parameters of the injector signal, their variation range and the values range of the corresponding resistor, together with the conversion formula to obtain the decimal value to provide to the digital potentiometer, are reported in Table 1.

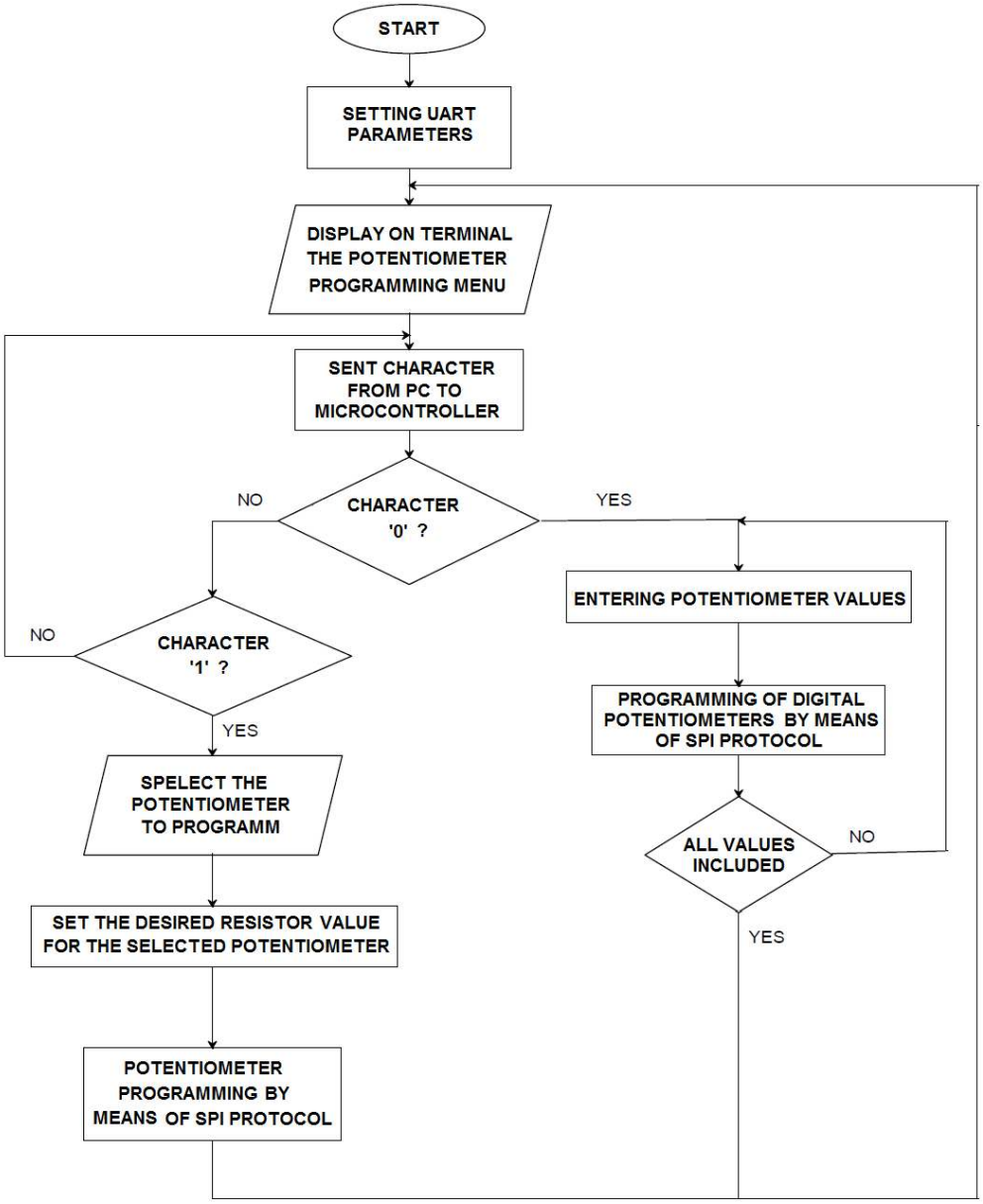

Figure 9. Flow chart of the developed firmware to program the potentiometer values.

Table 1. Conversion between the injection parameters and the potentiometer values.

Injection signal parameter	Electrical/ Temporal range	Resistance of mechanical potentiometer range	Conversion formula for digital potentiometer (Digital value)
Vstep up (R38)	42.5 V – 68.4 V	0 kΩ – 44 kΩ	$R38 = \left[\frac{V_{STEPUP} - 42.5}{0.115625} \right]$ (1)
Short Pulse (R40)	32.9µs – 172.9 µs	0kΩ – 20 kΩ	$R40 = \left[\frac{172.9 - T_{S.P.}}{1.372549} + 153 \right]$ (2)
Long Pulse (R29)	168 µs - 518 µs	0kΩ – 50 kΩ	$R29 = \left[\frac{T_{L.P.} - 168}{1.372549} \right]$ (3)
Toff (R24)	10.8 µs – 30.8 µs	0kΩ – 20 kΩ	$R24 = \left[\frac{T_{OFF} - 10.8}{0.196078} \right]$ (4)
Peack Current Threshold (R16)	10.25 A – 32.05 A	0kΩ – 10 kΩ	$R16 = \left[\frac{I_{P.C.T.} - 10.25}{0.08549} \right]$ (5)
Hold Current Threshold (R17)	7.15 A – 22.3 A	0kΩ – 10 kΩ	$R17 = \left[\frac{I_{H.C.T.} - 7.15}{0.05941} \right]$ (6)

The realised proto-board connected to a PC through a USB/RS232 adapter cable is shown in Figure 10(a), the connections between the digital potentiometers and connectors on the board in place of the removed mechanical potentiometers are shown in Figure 10(b). The realised driving system composed of the proto-board with digital programmable potentiometers, a PC for sending data for potentiometer programming and the injector driving board, was tested and the current and voltage waveforms were compared with those provided from the initial power board (with mechanical potentiometers).

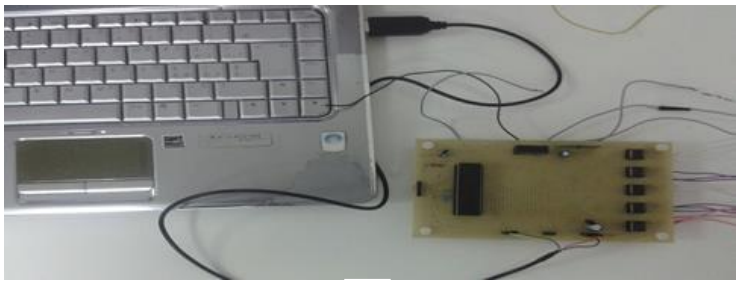

(a)

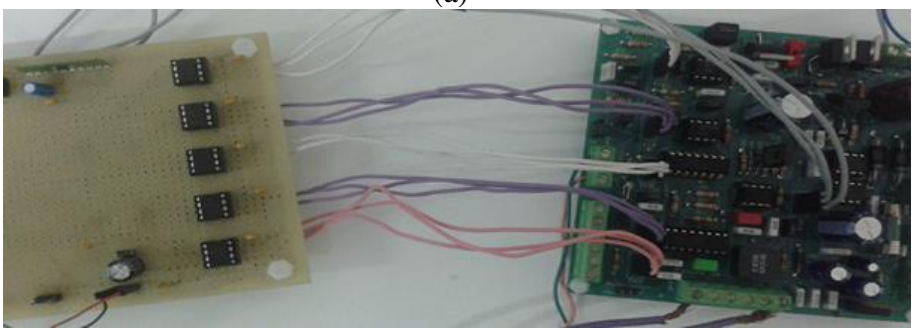

(b)

Figure 10. (a) Realised proto-board with digital potentiometers and PIC connected to a PC; (b) connections between the digital potentiometers and driving board.

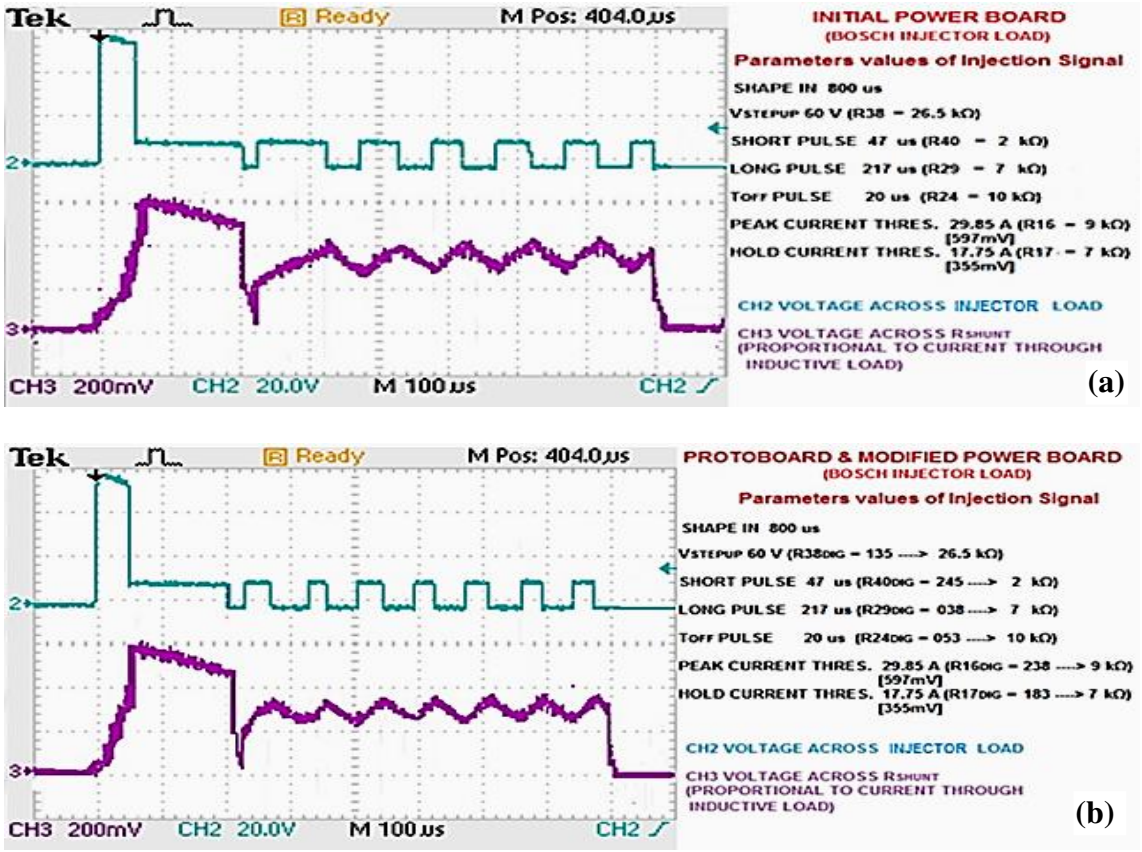

Figure 11. Trends of the driving signals using the Bosch injector and the new electronic board with digital potentiometers (b) similar to those provided from the initial power board (a).

Figure 12. Final aspect of the injectors driving unit placed into a branch box: rubberised bipolar cables were used for connecting the realised electronic system with the outside.

The voltage signal is taken on the R_{SHUNT} terminal (R_1 in Figure 4(b)) being proportional to the current flowing through the used Bosch injector. Figure 11(a) is relative to the captured signals employing the initial power board with mechanical potentiometers, whereas in Figure 11(b), the detected signals using the new driving solution are shown. With equal injection parameters, in one case defined manually and in the other by digital setting, waveforms are similarly confirming the proper operation of the implemented driving solution. Finally, the developed system for injector driving was assembled and placed inside a branch box with dimensions 30 × 20 × 12 cm^3 for better user management (as shown in Figure 12).

Experimental Procedure

Before analyzing the spray injections inside the velocimetric chamber, the necessary measures related to image acquisition, chamber illumination, synchronisation between signals and followed procedure to pass from one test to the next, are reported as follows. For image acquisition, the used system is composed of the following principal blocks: *optically accessible chamber* and *velocimetric camera (Memrecam GX-1F)* as described below. *Optically accessible chamber* (Figure 13): it is a steel chamber, with a parallelepiped shape, designed for a maximum pressure of 50 bar and provided with 4 accesses: 3 optical and 1 for the injector housing. One of the optical accesses, opposed to that for the injector housing, is aligned with the memrecam in order to capture the spray images. The chamber contains inert gas with a mean density similar to that of a typical motor in order to simulate the same conditions, in the combustion chamber, at injection start. An ambient temperature and quiescent gas conditions were adopted. In order to avoid fogging phenomena from the residual drops of the injected fuel, thus keeping clean the optical accesses, the chamber was continuously washed with fresh charge of inert gas even if, much more frequently, it was preferable to wait between one test and the next, in order to allow the fuel particles to deposit on the bottom of the chamber. In Figure 13, the velocimetric chamber used for the sprays injections (a) and injector tip inserted into the suitable access, on the opposite side to that of photo in Figure 13(b), are shown.

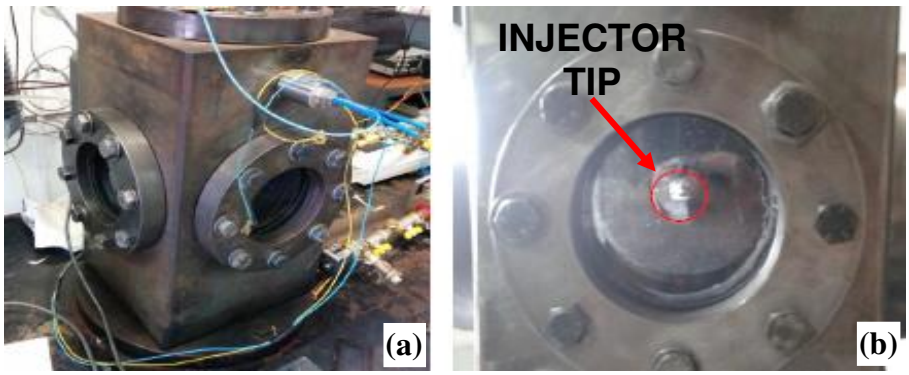

Figure 13. (a) View of the velocimetric chamber; (b) the injector tip into the chamber.

Velocimetric camera (Memrecam GX-1F): to properly acquire the images of the spray injections, the high speed camera was used. Figure 14(a) reports the memrecam aligned with the chamber optical access in order to acquire spray images, whereas a captured image displayed on a PC is shown in Figure 14(b). The camera has an acquisition frequency of 20 kHz (i.e. 20000 frames/sec), appropriate for the preset aims of our tests.

Using this frequency, it is possible to obtain an image resolution of 308 × 304 pixels thus being able to record up to 1.84 seconds (upper limit of the camera internal memory).

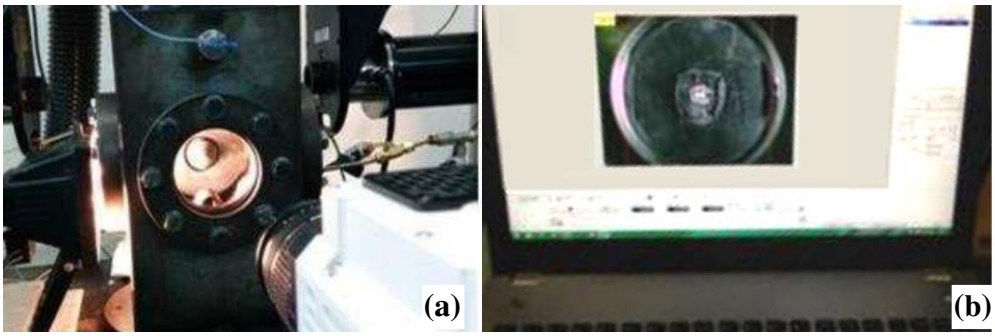

Figure 14. (a) Optical set-up with camera focusing on the injector tip into the velocimetric chamber; (b) GX-Link camera software interface on PC with the acquired image.

Afterwards, from the acquired image, it is necessary to extract the correct relation between pixel and mm, obtaining a scaling factor [pixel/mm] for proper post-processing. In order to clarify the adopted procedure for calculating the proper scaling factor between pixel and mm, which depends on the real dimension of the filmed objects with respect to the focus framing of the camera window (with dimension in pixel), a detailed description of the used procedure follows below. The initial photogram (without spray presence) was imported for each test, in *Autocad*, in a rectangular window with a dimension of 308×304 pixels; on this frame, the measured diameter (in pixel) of the injector tip was divided for the real dimension of the same tip (known value = 6.67 mm), thus obtaining the conversion coefficient. This procedure was adopted for each performed test and tests campaign because of possible slight shifts of the chamber during the conducted tests. Once the images have been acquired, another operation needs to be performed; considering the spray shape ratio defined as A/B, where A is the spray length and B is the rope with greater length in the perpendicular direction to A, the captured images from the camera show the spray projection in the orthogonal plane to injector axis. Therefore, to obtain the A value, the acquired penetration values must be divided for the sine of 71°, i.e. half angle of the injection cone (as reported in the injector datasheet). Furthermore, the light reflections caused by the chamber internal edges and injector tip did not allow to capture clean images; to improve the illumination level and to eliminate reflections, a black adhesive fabric layer type "mock velvet" was applied on the walls of the inside chamber. Instead, the injector tip was coated by software in the processing step using masks and filters with proper thresholds.

Memrecam Trigger Signal

The electronic unit provides the power signal to the injector when it receives the *Shape in the* signal, generated by the NI DAQ board. A train of eight pulses of the Shape-in signal was provided to the driving board, thus performing eight injections; to properly analyse the fuel injection images, the third and the fourth injection (named *pilot* and *main*), considered stabilised (with all the 5 sprays, even more important for low-pressure injections), were taken into account (Figure 15). Therefore, the delay of the camera triggering signal was set to capture from the third injection onward. Furthermore, the Bosch injector presents an intrinsic delay between the instants of the injection signal receiving and the injection start; considering the camera acquisition frequency of 20000

fps, the time shift Δt between two events, injection and recording, is among 0 and 50 µs. Thus, the first useful acquired frame was chosen as corresponding to the instant in which the injector tip appeared still closed; so the next acquired frame displayed the injection start with the spillage of fuel jets. Therefore, the event of the injector opening is located between the two cited frames. For obtaining the spray penetration curve, the effective instant of the injection start is important; to calculate the Δt time shift, the average penetration data related to one injection (5 sprays) were considered; through a polynomial regression of the second order, the best data interpolating function was found and by the intersection of this function with the time axis, the time shift was obtained.

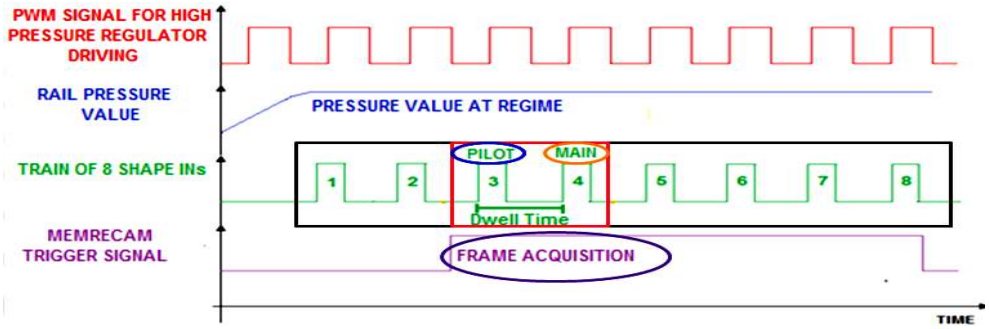

Figure 15. Signals for managing the system operation during a single injection test.

Image Post-processing

Once the spray images had been acquired, their quality was improved by removing reflections and imperfections, employing a digital photo retouching to provide to the LabVIEW software a better image quality useful for subsequent data processing and interpretation. The spray penetration mean value (i.e. distance between the injector tip and the spray ends), the standard deviation and shape ratio A/B of a single spray was determined, by using a suitable realised LabVIEW interface, for each acquired frame. A fundamental step, in this procedure, was the setting of the threshold values to determine a more accurate reconstruction of the spray morphology; an algorithm determines, for each image pixel, the spray presence or absence depending on the set threshold value. By using a lower or upper threshold, the image appeared in black or white colour; overlaying the same image processed with different thresholds (Figure 16(a)) and comparing the results with the original frame (in the upper corner on the left, Figure 16(b)), the proper threshold values were found.

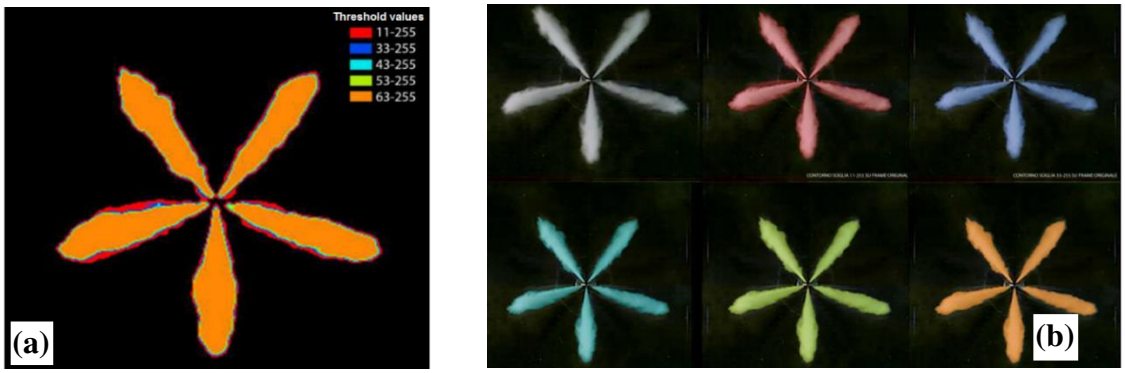

Figure 16. (a) Overlapping of the spray image with different threshold values; (b) original frame with beside different threshold values applied to the same frame.

High threshold values made it possible to obtain a spray morphology similar to that real, but when higher than necessary, sometimes, a spray division or narrowing in thin areas (such as that corresponding to injector tip) were generated. On the contrary, lower threshold values generated a more voluminous spray, giving as a result a possible merger in the tip area. Thus, a trade-off was found, assigning to the lower threshold value 33 and to the upper threshold, the value 255. Afterwards, once the proper sprays images were obtained, the error related to the derived thresholds was determined. This analysis was performed using a CAD program (by rescaling frames starting from the known value of the tip injector dimension) calculating the penetration of a single spray. By comparing these values with those obtained from the LabVIEW processing, the estimation error was found. The set values of the thresholds were used for each test, ensuring, in each frame, the presence of all the 5 sprays. After the described procedure, it was possible to display the images related to the development over time of the spray contours, the average penetration (inmmand pixels), standard deviation, spray shape ratio and number of the revealed sprays.

RESULTS AND DISCUSSION

The experimental tests were carried out by varying the injection pressure and the injector opening time for each tested fuel with a back-pressure value in the velocimetric chamber of 25 bar for all injection tests. In particular, the used settings are reported as follows:

i) Used fuels: diesel, biodiesel derived from coffee, from the Cynara cardunculus and Brassica carinata, each biodiesel blended with petroleum diesel in percentage equal to 20% , thus obtaining a B20 bio-diesel fuel.
ii) Fuel injection time (Energizing Time - ET) equal to 150, 300 and 450μs.
iii) Injection pressure equal to 500, 750, 1000 and 1250 bar.

The temperature was kept constant (ambient temperature) for each test; to ensure and verify the repeatability of the obtained results, each test was replicated two times. However, with 500 bar for the injection pressure and 150 μs for injector opening, it was not possible to detect the penetration and shape ratio values. Furthermore, the conversion factor was calculated for each test due to the possible minimal movements of the high speed camera or some apparatus connected to it, such as the easel. In fact, between one test and the other one, the calibration operations (i.e. back-pressure control inside the chamber or washing of optical access) were performed with possible movements of the chamber/camera position. Nevertheless the calculated conversion factors for the same test repeated twice and for the same tested fuel these are very similar. The results relative to the sprays' average penetration and to the standard deviation, obtained varying the injector pressure and opening time (ET), are reported in the following graphs for all the tested fuels.

The graphs, shown in Figure 17, report the average penetration values relative to the 5 sprays of the injection. As shown in Figure 17(a), for an injection pressure equal to 750 bar, the bio-diesel fuels derived from the Brassica carinata and Cynara cardunculus exhibit a penetration of about 10mm, much greater compared to the other types of fuels (exactly 8 mm for biodiesel derived from coffee and lower than 6 mm for conventional petroleum diesel). With an injection pressure equal to 1000 bar, the penetration is higher reaching about 12 mm for coffee, about 11mm for Brassica carinata and Cynara cardunculus bio-diesels and about 8mm for petroleum diesel (Figure 17(b)). Upon increasing the injection pressure, the average penetration values are equal to about 10mm

for all tested fuels except for Cynara cardunculus that reaches an average penetration value of 12 mm. As found in the performed experimental tests, biodiesel fuels, being characterised by a slightly greater density and viscosity than petroleum diesel, reach a higher penetration inside the velocimetric chamber. On the contrary, the obtained penetration features, as reported in De Domenico et al. [23], are slightly different (i.e. standard diesel fuel and Cardoon with a slightly higher spray penetration compared to the Brassica one), but using B100 biofuels differently from the B20 fuel blends used in this work, as discussed in the introduction.

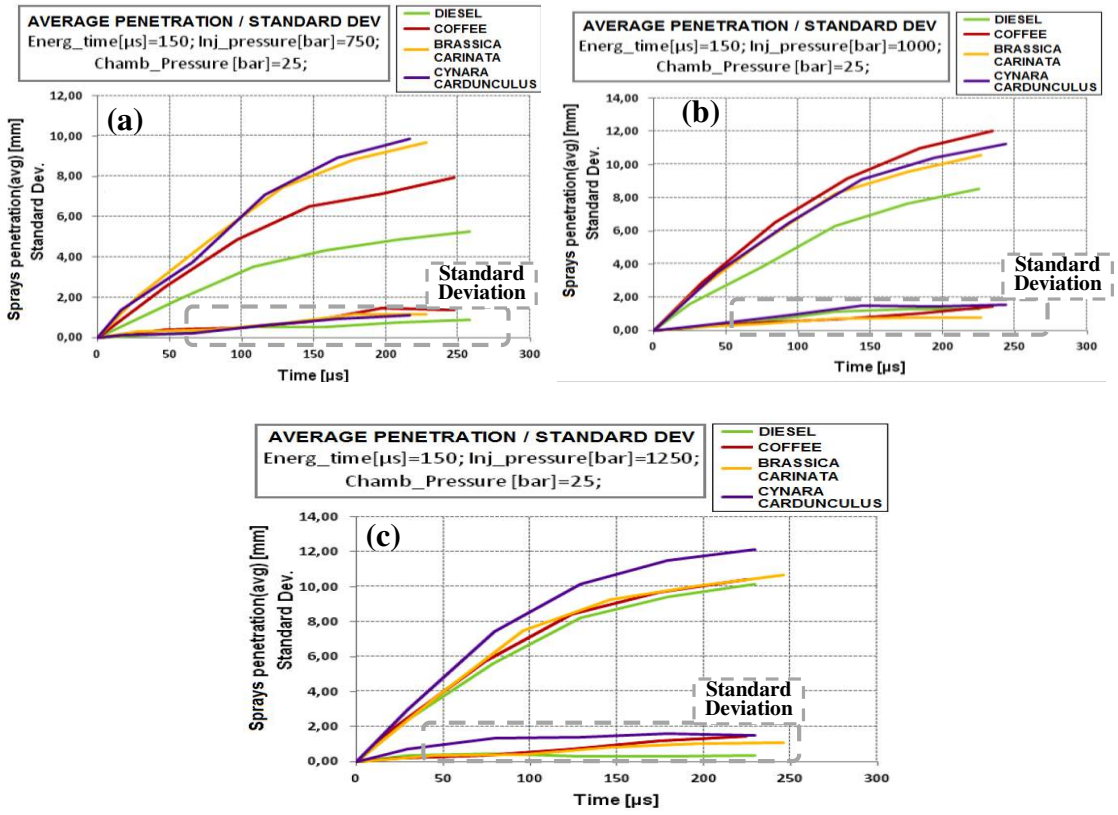

Figure 17. Graphs relative to the sprays penetration for different injector pressure values, i.e. 750 bar (a), 1000 bar (b), 1250 bar (c) with ET= 150 µs, concerning all tested fuels.

The following graphs, shown in Figure 18, report the average penetration values of the injected fuel sprays and the standard deviation using an injection opening time of 300 µs. In this case, the average penetration reaches higher values compared to the previous tests (with an injection opening time of 150 µs), for all tested fuels. In fact, in Figure 18(a), relative to an injection pressure of 500bar, the sprays average penetration reaches 14mm for biofuels derived from Cynara cardunculus, 13 mm for Brassica carinata and coffee-based ones and about 10 mm for the conventional petroleum diesel. Upon increasing the injection pressure value to 750 bar (Figure 18(b)), for biodiesel fuels derived from Cynara cardunculus and coffee, an average penetration greater than 18 mm was reached, whereas about 17 mm for the Brassica carinata-based one and about 15 mm using conventional diesel fuel. For an injection pressure value of 1000 bar, the average penetration values of the injected sprays increase up to 22 mm for the Cynara cardunculus-based bio-diesel, 20mm for coffee and Brassica carinata based ones and up

to 17 mm for petroleum diesel (Figure 18(c)). Using an injector pressure value of 1250bar, the average penetration values increase for all tested fuels and the difference between these values is lower, as reported in Figure 18(d); in particular, for the B20 biodiesel derived from Brassica carinata, an average penetration of about 26mm was reached, about 24mm using the Cynara cardunculus based one, 23 mm for biodiesel from coffee and 22mm for diesel. Therefore, as expected, greater injection pressure values lead to an increase of the spray penetration; moreover the, curves of Figures 17 and 18 for different ET values show that the penetration increases more linearly varying the opening time rather than the injection pressure.

Figure 19 reports the injection tests with an injector opening time of 450 µsec whereas other parameters remain unchanged from the previously performed tests (e.g chamber pressure = 25 bar). With an injection pressure of 500 bar, the average penetration of the injected sprays using the Cynara cardunculus based biodiesel reaches an additional 24 mm than the 20 and 19 mm reached with Brassica carinata and coffee based biodiesel fuels respectively; a slightly lower value instead is obtained for petroleum diesel (18 mm). Upon increasing the pressure up to 750 bar, the three biodiesel fuels reach an average penetration of ≈26-27 mm (Figure 19(b)) whereas diesel penetration is equal to 23 mm. With an injection pressure equal to 1000 bar (Figure 19(c)), the sprays penetration of biodiesels rises up to 30 mm; for diesel instead it is about 24 mm. For the last test with injector pressure = 1250 bar, the sprays penetration of biodiesels reaches 33-34 mm and about 30mm for the petroleum diesel (Figure 19(d)). As previously reported for the plots of Figures 17 and 18, also for the curves of Figure 19, the spray penetration increases more linearly varying the opening time rather than the injection pressure.

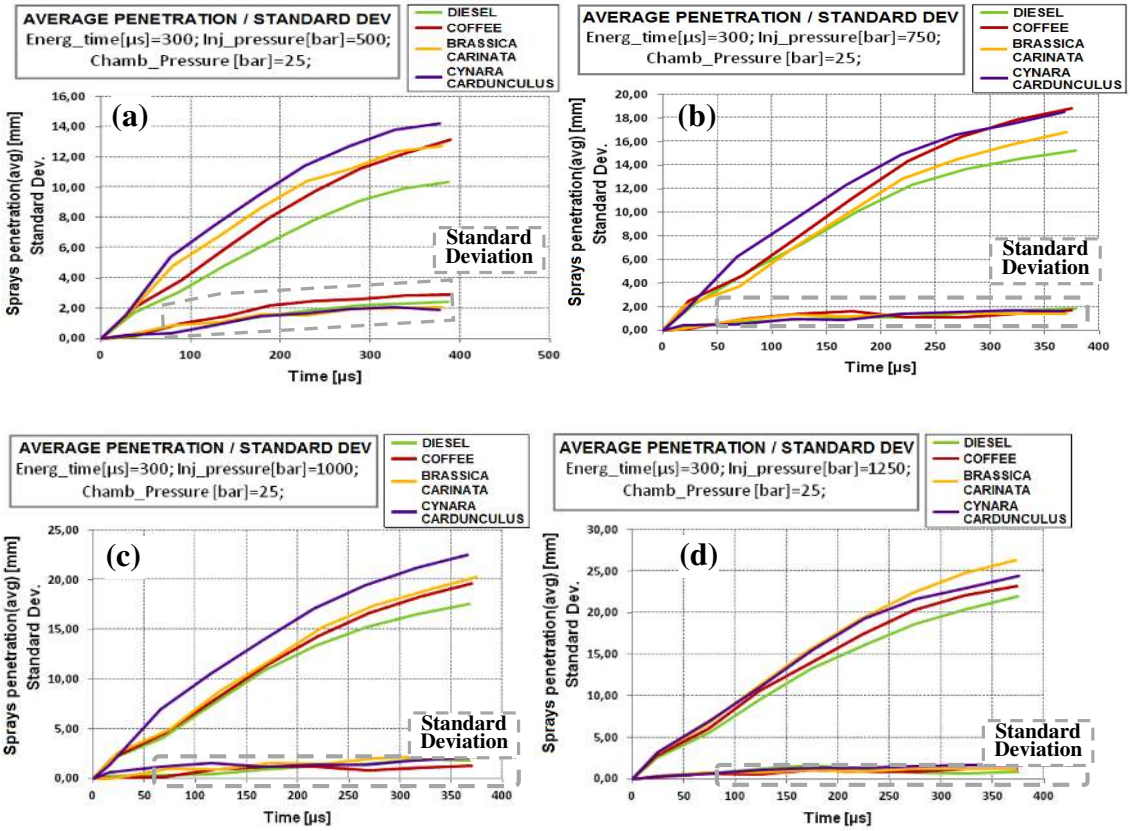

Figure 18. Sprays average penetration and standard deviation related to all tested fuels with injector opening time (ET) of 300µs and different values of the injection pressure.

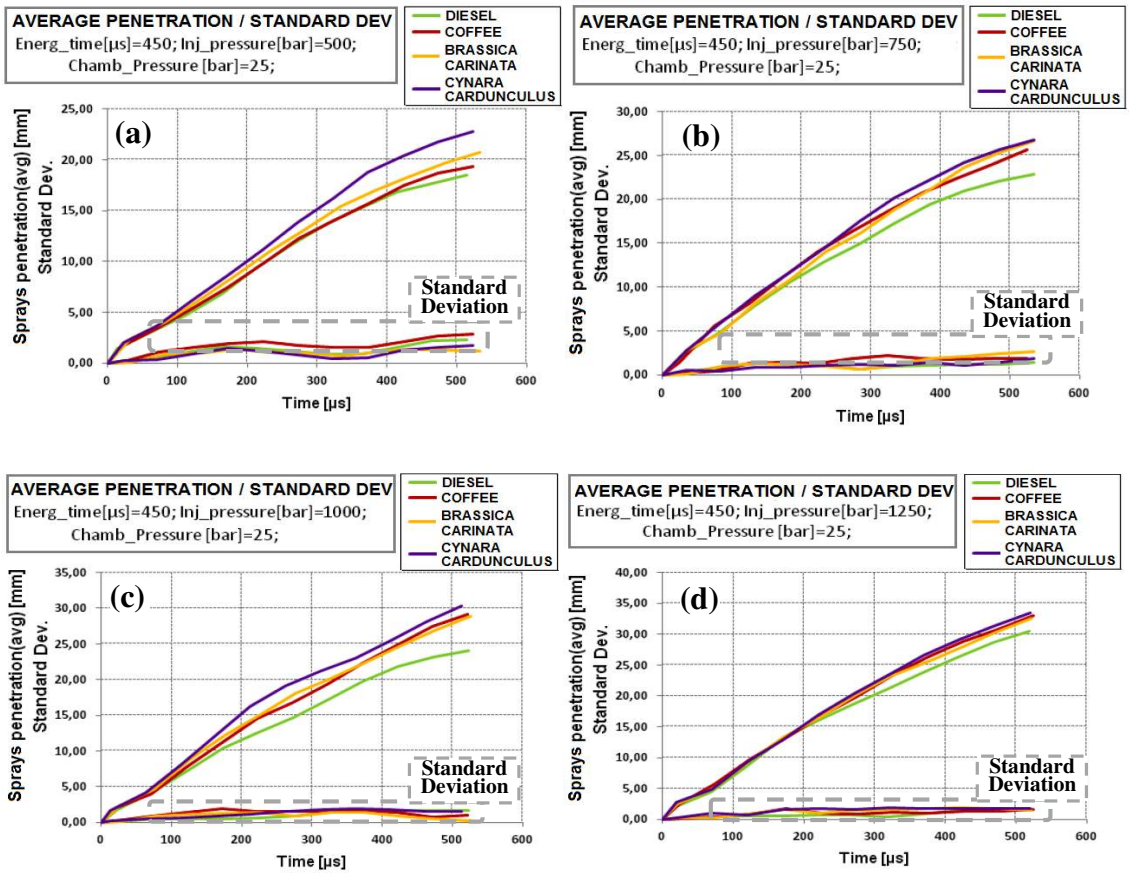

Figure 19. Graphs related to the injector opening time (ET) of 450 µs; the average penetration is higher, for all tested fuels, compared to the previous tests with shorter ET values.

The obtained results are also confirmed by other research works [28-35]. For example, in Sathrudhan et al. [28-35], the simulations were carried out using different nozzle diameters (0.15, 0.2, 0.3) mm, varying pressure between 800,1200 and 1800 bar values and the fuel typology, i.e. standard diesel, *Rapemethyl Ether* (RME) and *Dimethyl Ether* (DME), each of them featured by different fluid properties. The DME spray spreads widely with short penetration, being less dense than diesel, hence the liquid portion of the DME spray has shorter penetration than the diesel one. On the contrary, the RME penetrates more when compared to diesel and DME, because of large droplets and a higher mass density. Summarising our obtained experimental results, by increasing the injector pressure, as expected, a higher average penetration value is obtained due to a greater initial velocity and thus higher quantity of motion of the injected fuel. In particular, observing the shape of each penetration curve, it is possible to notice peculiar characteristics regarding three different curve sections, for all performed tests:

i) The first section with a steep gradient and linear behaviour over time is related to injection in the first time instants; in this phase, the chamber back-pressure is still weak and the jet is compact, essentially governed by only the injector pressure.
ii) The second curve section presents a *knee* shape; in this phase, the injection interacts significantly with the back-pressure chamber determining a deceleration of the spray penetration. The drops larger than others accumulate energy on the outer surface that

causes, beyond a certain limit of instability, the breaking and the formation of smaller droplets. The *knee* value is referred to in the literature as the *break up length.*

iii) The third section shows a typical root square dependence over time; the injection tends to a steady-state condition with a strong reduction of the spray penetration velocity.

Concerning the qualitative aspect, no significant difference appears between the values related to the B20 biodiesel and diesel fuels; anyway, upon varying the injection pressure, for conventional diesel it results in a minor penetration compared to that of the used biodiesel fuels. The reason has to be found in the biodiesel chemical/physical properties; in fact, although used biodiesels contain only 20% of renewable vegetable-origin biofuel, their viscosity and superficial tension are higher than those of petroleum diesel. Therefore, due to a weak vaporisation with the consequent formation of drops with a larger diameter, the sprays penetration for biodiesel fuels reaches higher values than in the case of conventional diesel.

To complete the discussion about the reached results, an anomaly concerning the penetration inhomogeneity of the individual sprays, related to a single injection, has to be mentioned. This inhomogeneity appeared specially in the first injection instants, also reducing almost fading away as the injection pressure increases. This phenomenon is related to sporadic cases because, in order to make a test as reliable as possible, the injection images were captured from the third injection, allowing the injection process to achieve a certain stationarity and stability. For example, considering an injection test with ET = 300 μs and an injection pressure of 500 bar (Figure 18(a)), some fuels, such as biodiesel derived from coffee, present a standard deviation curve that exceeds the value of 2 almost reaching 3. This means that a certain non-uniformity among the 5 jets of the same injection occurs, resulting in two jets shorter compared to the other three. In conclusion, Siebers [50] reports that the injection pressure, considering the injected sprays of conventional diesel, has no significant effect on the liquid-phase penetration of the spray itself. On the contrary, as reported in De Domenico et al. [18], upon varying injection pressure, a slight increase of the spray penetration is obtained, but this is much lower than the opening time effect. In our research work, as obtained by the experimental curves and a qualitative analysis on the quantification of effects, it results that the penetration value is mostly influenced by the opening time (i.e. *Energizing time*, ET) rather than the injection pressure. As an example, considering an ET of 300μs and injection pressure that doubles from 500 to 1000 bar, the spray penetration increases to 41.2% for conventional diesel, to 35.0% for coffee and Brassica carinata and to 37.7% for the Cynara cardunculus biofuel. On the other hand, by doubling the opening time (ET from 150 to 300 μs), with a constant injection pressure of 1000 bar, the spray penetration increases to 50.2% for diesel (9% more than the increase due to the injection pressure doubling), 40.0% for coffee biodiesel (with a 5% more), 47.5% for Brassica carinata (12.5% more) and finally 51.1% for Cynara cardunculus (13.4% more than the increase due to the injection pressure doubling). This trend is also respected for other values of the opening time (ET) and injection pressure, confirming that the Energizing time has a greater influence on the penetration value of the injected sprays than the injection pressure.

CONCLUSIONS

In this work, an experimental apparatus was realised in order to perform a morphological characterisation of the sprays injection of different fuel types. Using this setup, tests were carried out to analyse the sprays evolution and penetration inside a velocimetric chamber

provided with optical accesses used to record the process; a Bosch injector, driven by a suitable realised electronic system, was used. The sprays penetration employing different fuel typologies, such as the B20 biodiesel derived from Cynara cardunculus, from Brassica carinata and from coffee and conventional petroleum diesel, was analysed setting, for each test and fuel, different parameters such as the injector pressure and the injection opening time while maintaining constant the back-pressure value inside the velocimetric chamber. The results show a deeper penetration for all biodiesel fuels compared to conventional diesel due to the different biodiesel chemical/physical properties such as higher viscosity and superficial tension, with the consequent formation of drops with a larger diameter, with respect to conventional diesel. Furthermore, it results that the penetration value is mostly influenced by the opening time rather than by the injection pressure. The realised programmable electronic system has proved to be able to drive correctly the diesel injector making it possible to adjust, as desired by the user or required by a specific application, the injector pressure and the opening time. Therefore, the designed system is a good candidate to be applied in test benches where the injector parameters have to be adjusted for carrying out the morphological analysis of biofuels sprays and for optimising the injector operation. Furthermore, the reported results, concerning the sprays morphological analysis of the tested biofuels, can be used by future research works for obtaining the desired injection parameters thus improving engine performance and fuel consumption.

REFERENCES

[1] Hoque N, Mourshed M, Das BK. Performance and emission comparison of Karanja (pongamia pinnata), Pithraj (aphanamixis polystachya), Neem (azadira chtaindica) and Mahua (madhuca longofolia) seed oil as a potential feedstock for biodiesel production in Bangladesh. International Journal of Automotive and Mechanical Engineering. 2015;12:2967-82.

[2] Sarah AG, Rajanikanth BS. NOx Reduction from Biodiesel Exhaust by Plasma Induced Ozone Injection Supported by Lignite Waste Adsorption. IEEE Transactions on Dielectrics and Electrical Insulation. 2016;23:2006-14.

[3] Pushparaj T, Venkatesan C, Ramabalan S. Emission Studies on Karanja Biodiesel Fuelled Diesel Engine with Ethanol as Additive. IEEE-International Conference On Advances In Engineering, Science And Management2012. p. 263-8.

[4] Azad AK, Rasul, MG, Giannangelo B, Islam R. Comparative study of diesel engine performance and emission with soybean and waste oil biodiesel fuels. International Journal of Automotive and Mechanical Engineering. 2015;12:2866-81.

[5] Hasan MM, Rahman MM, Kadirgama K. A Review on homogeneous charge compression ignition engine performance using biodiesel–diesel blend as a fuel. International Journal of Automotive and Mechanical Engineering. 2015;11:2199-211.

[6] Habib M, Ul Haq I, Mustafa P, Rehman H, Khan R, Ullah Khan A. Production of biofuels from micro ALGAE and green wastes through Anaerobic Digestion. Power Generation System and Renewable Energy Technologies. Islamabad, Pakistan; 2015.

[7] Ahamed JU, Raiyan MF, Hossain MS, Rahman MM, Salam B. Production of biogas from anaerobic digestion of poultry droppings and domestic waste using

catalytic effect of silica gel. International Journal of Automotive and Mechanical Engineering. 2016;13:3503 - 17.

[8] Kamil M, Rahman MM, Bakar RA, Kadirgama K. Modeling of SI engine for duel fuels of hydrogen, gasoline and methane with port injection feeding system. Energy Education Science and Technology Part A: Energy Science and Research. 2012;29:1399-416.

[9] Shukri MR, Rahman MM, Ramasamy D, Kadirgama K. Artificial neural network optimization modeling on engine performance of diesel engine using biodiesel fuel. International Journal of Automotive and Mechanical Engineering. 2015;11:2332-47.

[10] Hiltunen E, Salminen HJ, Niemi S, Pasila A, Vauhkonen V. Production of bio-oils: physical and energy technical properties. International Conference on Clean Electrical Power; 2007. p. 406-8.

[11] Carlucci AP, Colangelo G, Ficarella A, Laforgia D, Strafella L. Improvements in dual fuel biodiesel producer gas combustion at low loads through pilot injection splitting. Journal of Energy Engineering. 2015;141:061-8.

[12] Kapilan N, Ashok Babu TP, Reddy RP. Improvement of performance of dual fuel engine operated at part load. International Journal of Automotive and Mechanical Engineering. 2010;2:200-10.

[13] Azad AK, Ameer Uddin SM, Alam MM. A comprehensive study of DI diesel engine performance with vegetable oil: an alternative bio-fuel source of energy. International Journal of Automotive and Mechanical Engineering. 2012;5:576-86.

[14] Hoque N, Mourshed M, Das BK. Performance and emission comparison of Karanja (pongamia pinnata), Pithraj (aphanamixis polystachya), Neem (azadira chtaindica) and Mahua (madhuca longofolia) seed oil as a potential feedstock for biodiesel production in Bangladesh. International Journal of Automotive and Mechanical Engineering. 2015;12:2967-82.

[15] Rizwanul Fattah IM, Kalam MA, Masjuki HH, Wakila MA. Biodiesel production, characterization, engine performance, and emission characteristics of Malaysian Alexandrian laurel oil. RSC Advances. 2014;4:17787-96.

[16] Wakil MA, Masjuki HH, Kalam MA, Teoh YH, How HG, Imtenan S. Influence of engine operating variable on combustion to reduce exhaust emissions using various biodiesels blend. RSC Advances. 2015;5:100674–81.

[17] Zhao J, Wang J. Adaptive observer for joint estimation of oxygen fractions and blend level in biodiesel fueled engines. IEEE Transactions on Control Systems Technology. 2015;23:80-90.

[18] Hamada KI, Rahman MM, Ramasamy D, Noor MM, Kadirgama K. Numerical investigation of in-cylinder flow characteristics of hydrogen-fuelled internal combustion engine. Journal of Mechanical Engineering and Sciences. 2016;10:1782-80.

[19] Said NH, Ani FN, Said MFM. Review of the production of biodiesel from waste cooking oil using solid catalysts. Journal of Mechanical Engineering and Sciences. 2015;8:1302-11.

[20] Arnesano M, Carlucci AP, Laforgia D. Extension of portfolio theory application to energy planning problem – The Italian case. Energy. 2011;39:112-24.

[21] Ronde H, Ranne A, Pursiheimo E. Integrated renewable energy solutions for seafood processing stations. Proc of International Conference on Energy and Sustainable Development: Issues and Strategies; 2010.

[22] Carlucci AP, Ficarella A, Strafella L, Tricarico A, De Domenico S, D'Amico L, Santino A. Behaviour of a compression ignition engine fed with biodiesel derived from cynara cardunculus and coffee grounds. Proc of 37th Meeting of the Italian Section of the Combustion Institute; 2015.

[23] De Domenico S, Strafella L, D'Amico L, Mastrorilli M, Ficarella A, Carlucci PA, Santino A. Biodiesel production from Cynara cardunculus L. and Brassica carinata A. Braun seeds and their suitability as fuels in compression ignition engines. Italian Journal of Agronomy. 2016;11:47-56.

[24] Ricco M, De Matthaeis S, Olabi AG. Simulation of the magnetic properties for common rail electro-injector. Journal of Materials Processing Technology. 2004;155:1611-5.

[25] Saponaro F, Lino P, Maione G. A dynamical model of electro-injectors for common rail diesel engines. 22nd Mediterranean Conference on Control and Automation. University of Palermo, Italy; 2014. p. 207-2011.

[26] Visconti P, Ventura, V., Carlucci, A. P., Strafella, L. Driving electronic board with adjustable piloting signal parameters for characterization of Common Rail diesel injectors with pure biodiesel. IEEE 16th International Conference on Environment and Electrical Engineering. Florence, Italy2016.

[27] Kamil M, Rahman MM. Effect of injection hole diameter on operational conditions of common-rail fuel-injection system for portinjection hydrogen-fueled engine. International Journal of Automotive and Mechanical Engineering. 2015;11:2383-95.

[28] Sathrudhan Choudhary V, Pradeepkumar C, Ramkumar A. Spray Characteristic Analysis Of Diesel Injector with Biodiesel. International Journal of Research and Innovation in Engineering Technology. 2015;2:1-9.

[29] Battistoni M, Grimaldi CN. Numerical analysis of injector flow and spray characteristics from diesel injectors using fossil and biodiesel fuels. Applied Energy. 2012;97:656-66.

[30] Carlucci AP, Panarese N, Laforgia D. Experimental characterization of diesel fuel pulsed sprays. SAE Technical Paper 2007.

[31] Agarwal AK, Gupta JG, Maurya RK, Kim W, Lee S, Lee CS, Park, S. Spray evolution, engine performance, emissions and combustion characterization of Karanja biodiesel fuelled common rail turbocharged direct injection transportation engine. International Journal of Engine Research. 2016;17:1092-107.

[32] Carlucci AP, Ficarella A, Laforgia D. Potentialities of a common rail injection system for the control of dual fuel biodiesel-producer gas combustion and emissions. Journal of Energy Engineering. 2014;140:A4014011-1A-8.

[33] Kettner M, Dechent S, Hofmann M, Huber E, Arruga H, Mamat R, et al. Investigating the influence of water injection on the emissions of a diesel engine. Journal of Mechanical Engineering and Sciences. 2016;10:1863-81.

[34] Robert J. Best JMK, Morrow JD, Fox B. Steady-State and transient performance of biodiesel-fueled compression-ignition-based electrical generation. IEEE Transactions On Sustainable Energy. 2011;2:20-7.

[35] Uludamar E, Tüccar G, Aydın K, Özcanlı M. Vibration analysis of a diesel engine fuelled with sunflower and canola biodiesels. Advances in Automobile Engineering. 2016;5(1):1-5.

[36] Kamil M, Rahman MM. Effect of injection hole diameter on operational conditions of common-rail fuel-injection system for port-injection hydrogen-

fueled engine. International Journal of Automotive and Mechanical Engineering. 2015;11:2383-95.

[37] Deeparaja E, Viveka B, Gunasekarana D, Satheeshkumara N, Magudeswaranb M, Srinivasanb SA. Spray characteristic analysis of diesel injector with biodiesel. South Asian Journal of Engineering and Technology. 2016;2:195-205.

[38] Farooqi QR, Snyder, B., Anwar, S. Real Time Monitoring of Diesel Engine Injector Waveforms for Accurate Fuel Metering and Control. Journal of Control Science and Engineering. 2013;2013:1-9.

[39] Carlucci AP, Ficarella A, Laforgia D, Trullo G. Multiobjective optimization of the breathing system of an aircraft two stroke supercharged Diesel engine. Energy Procedia.2015;82:31-7.

[40] Liao CJ, Mi L, Pontrelli S, Luo S. Fuelling the future: microbial engineering for the production of sustainable biofuels. Nature Reviews Microbiology. 2016;14:288-304.

[41] Ghafoori M, Ghobadian B, Najafi G, Layeghi M, Rashidi A. and Mamat R. Effect of nano-particles on the performance and emission of a diesel engine using biodiesel-diesel blend. International Journal of Automotive and Mechanical Engineering. 2015;12:3097-108.

[42] Carlucci AP, Laforgia D, Saracino R, Toto G. Combustion and emissions control in diesel–methane dual fuel engines: The effects of methane supply method combined with variable in-cylinder charge bulk motion. Energy Conversion and Management. 2011;52:3004-17.

[43] Carlucci AP, Laforgia D, Motz S, Saracino R, Wenzel SP. Advanced closed loop combustion control of a LTC diesel engine based on in-cylinder pressure signals. Energy Conversion and Management. 2014;77:193-207.

[44] Carlucci AP, Visconti P, Primiceri P, Strafella L, Ficarella A, Laforgia D. Photo-induced ignition of different gaseous fuels using carbon nanotubes mixed with metal nanoparticles as ignitor agents. Combustion Science and Technology. 2016; 189(6): 937-953.

[45] Donateo T, Carlucci AP, Strafella L, Laforgia D. Experimental validation of a cfd model and an optimization procedure for dual fuel engines. SAE International. SAE Technical Paper 2014-01-13142014.

[46] Primiceri P, Visconti P, Melpignano A, Colleoni G, Vilei A. Hardware and software solution developed in arm MBED environment for driving and controlling DC brushless motors based on ST X-Nucleo development boards. International Journal on Smart Sensing and Intelligent Systems. 2016;9:1534-62.

[47] Primiceri P, Visconti P, Longo D, Tramis R, Carlucci AP. Design and testing of user-configurable driving boards of pulsed xenon lamps with adjustable flash duration and brightness for carbon-nanotubes photo-induced ignition. Journal of Engineering and Applied Sciences. 2016;11:12336-42.

[48] De Giorgi MG, Sciolti A, Campilongo S, Ficarella A. Image processing for the characterization of flame stability in a non-premixed liquid fuel burner near lean blowout. Aerospace Science and Technology. 2016;49:41-51.

[49] Sathiyamoorthi R, Sankaranarayanan G. Fuel injection timings of a direct injection diesel engine running on neat lemongrass oil-diesel blends. International Journal of Automotive and Mechanical Engineering. 2015;11:2348-63.

[50] Siebers D. Liquid-Phase Fuel Penetration in Diesel Sprays. SAE Technical Paper. 9808091998.